

# On the benefits of localized modes in anharmonic vibrational calculations for small molecules

Paweł T. Panek, Christoph R. Jacob<sup>1</sup>

TU Braunschweig,  
Institute of Physical and Theoretical Chemistry,  
Hans-Sommer-Str. 10, 38106 Braunschweig, Germany

Date: May 04, 2016

Status: *J. Chem. Phys.* **144**, 164111 (2016).

DOI: 10.1063/1.4947213

---

<sup>1</sup>E-Mail: c.jacob@tu-braunschweig.de

## Abstract

Anharmonic vibrational calculations can already be computationally demanding for relatively small molecules. The main bottlenecks lie in the construction of the potential energy surface and in the size of the excitation space in the vibrational configuration interaction (VCI) calculations. To address these challenges, we use localized-mode coordinates to construct potential energy surfaces and perform vibrational self-consistent field (L-VSCF) and L-VCI calculations [P. T. Panek, Ch. R. Jacob, *ChemPhysChem* **15**, 3365 (2014)] for all vibrational modes of two prototypical test cases, the ethene and furan molecules. We find that the mutual coupling between modes is reduced when switching from normal-mode coordinates to localized-mode coordinates. When using such localized-mode coordinates, we observe a faster convergence of the  $n$ -mode expansion of the potential energy surface. This makes it possible to neglect higher-order contributions in the  $n$ -mode expansion of the potential energy surface or to approximate higher-order contributions in hybrid potential energy surfaces, which reduced the computational effort for the construction of the anharmonic potential energy surface significantly. Moreover, we find that when using localized-mode coordinates, the convergence with respect to the VCI excitation space proceeds more smoothly and that the error at low orders is reduced significantly. This makes it possible to devise low-cost models for obtaining a first approximation of anharmonic corrections. This demonstrates that the use of localized-mode coordinates can be beneficial already in anharmonic vibrational calculations of small molecules, and provides a possible avenue for enabling such accurate calculations also for larger molecules.

# 1 Introduction

Going beyond the harmonic approximation in theoretical vibrational spectroscopy is an important step, as it gives access to chemically accurate spectroscopic and thermochemical data. With some effort, for small-to-medium size molecules a quantitative agreement with experimental results can be achieved.<sup>[1–3]</sup> There are two major well-established approaches for calculations of anharmonic vibrational spectra, vibrational perturbation theory (VPT) and variational methods. In the first one, the anharmonicity is treated as a perturbation of the zeroth-order solution obtained in the harmonic approximation.<sup>[4,5]</sup> In the latter approach, on which we will focus here, the nuclear Schrödinger equation is solved in a variational manner, analogously to electronic structure methods. Most prominent starting-point is the vibrational self-consistent field (VSCF) method, on top of which the lacking vibrational correlation energy is approximated by methods such as vibrational configuration interaction (VCI) or (non-variational) vibrational coupled cluster (VCC) theory.<sup>[6,7]</sup>

However, all available approaches are feasible only for relatively small molecules. The first bottleneck lies in constructing the anharmonic potential energy surface (PES). Mapping the full PES directly for all vibrational coordinates is achievable only for molecules consisting of few atoms, as the number of required grid points grows exponentially with the number of nuclei. In VPT, the PES is thus approximated by a Taylor expansion of the energy at the equilibrium geometry, which is usually truncated at third or fourth order. On the other hand, variational methods usually employ a truncated  $n$ -mode expansion<sup>[8,9]</sup> of the PES, in which the potential energy is expanded discretely on a grid. An accurate approximation of the PES requires the inclusion of higher-order terms in the  $n$ -mode expansion. The main hindrance in the  $n$ -mode expansion is the need for the calculation of coupling terms, i.e., of two-mode, three-mode, or even higher-order potentials.

Several methods have been developed to speed up the construction of the PES and in order to make anharmonic vibrational calculations feasible also for larger systems. For some combinations of modes, the couplings will be relatively small, which could be prescreened without a significant loss of accuracy.<sup>[10-14]</sup> Another possibility to tackle the computational cost of obtaining the higher-order terms in the PES expansion are multi-level or hybrid approaches,<sup>[12,15,16]</sup> in which electronic-structure methods of different levels are applied to the different terms of the PES expansion. In the spirit of an hierarchical expansion, the most dominant one-mode terms are treated with high-level electronic-structure methods, such as coupled-cluster theory, whereas for the two-mode or higher-order terms less accurate but more efficient methods, such as density-functional theory, are employed.

Since VSCF describes the interaction of modes only in a mean-field manner, post-VSCF methods such as VCI<sup>[17]</sup> have to be applied to recover the vibrational correlation energy. Here, the main computational bottleneck arises from the construction of the VCI-Hamiltonian matrix. Its size depends on the expansion of the VCI space. Converged VCI energies require rather large excitation spaces, which again limits the applicability of the method to small molecules. This problem is addressed with several configuration selection methods, where only the mostly contributing states are included in the VCI expansion, vastly reducing the size of the Hamiltonian.<sup>[18-21]</sup>

Thus, in general there are three main aspects that need to be addressed to make anharmonic vibrational calculations feasible for larger molecules: (i) the convergence of the  $n$ -mode expansion and therein (ii) the possibility to neglect or approximate some of the couplings between modes, and (iii) the convergence of the expansion of the excitation space in the post-VSCF treatment, namely the VCI space. The choice of coordinates, in which the calculations are performed, will affect all three of these aspects. Here, we will explore to what extent a suitable choice of the coordinates can be beneficial for anharmonic vibrational calculations. In the present study, we will focus on rectilinear

coordinates. Curvilinear coordinates, though more natural, imply a more complicated form of the kinetic energy operator, which in turn makes the solution of the vibrational Schrödinger equation more demanding.<sup>[22–25]</sup>

Normal-modes coordinates, obtained in the harmonic approximation, are the most common choice for anharmonic vibrational calculations. Unfortunately, in the anharmonic regime they provide a complicated picture of strong couplings between the normal modes. This results in a slow convergence, both with respect to the  $n$ -mode expansion of the PES, and with respect to the VCI-expansion of the excitation space.

One way of defining more appropriate coordinates are so-called local modes.<sup>[26]</sup> They arise from the assumption that X–H stretching vibrations, instead of being collective motions of many X–H groups should rather be a set of coupled single-bond stretching motions, and such strictly local vibrational coordinates are thus constructed. Such local modes were successfully applied to O–H stretching vibrations of water clusters and alcohols, giving access to overtone spectroscopy.<sup>[27–29]</sup> A special case of local modes is the local monomer model (LMon) presented by Bowman and coworkers.<sup>[30–32]</sup> The FALCON scheme by König *et al.* constructs strictly local vibrational coordinates in a similar spirit.<sup>[33]</sup>

Another approach are optimized coordinates, which are obtained from a transformation of the normal modes coordinates during the VSCF procedure to minimize the VSCF energy.<sup>[34,35]</sup> Yagi and coworkers introduced optimized-coordinate variants of VSCF, VCI, and VCC and showed that in the new basis a faster convergence with respect to the excitation space is observed.<sup>[36,37]</sup> These coordinates were also employed in a post-VSCF perturbative treatment.<sup>[38]</sup> It was noticed that the optimization procedure can provide coordinates that are well localized, and thus mutually decoupled. However, in this framework a full quartic force field is used and transformed during the optimization, which precludes computational savings in the construction of the PES.

The locality of the coordinates can also be enforced during a transformation of normal modes coordinates. Such rigorously defined localized modes have been introduced for the analysis and interpretation of selected bands of vibrational spectra of large molecules.<sup>[39–44]</sup> We have previously developed localized-modes variants of VSCF and VCI, termed L-VSCF and L-VCI, respectively.<sup>[45]</sup> For selected vibrations of water clusters and polypeptides, we could show that localized-mode coordinates lead to an organized picture of the couplings between the localized modes, allowing for neglecting some of the coupling potentials *a priori*, without a loss in accuracy. Moreover, a faster convergence within the VCI excitation space was observed. Cheng and Steele applied such localized-modes coordinates only in the VSCF framework, and explored using distance-based criteria for neglecting two-mode couplings.<sup>[46]</sup> Hanson-Heine investigated the harmonic couplings arising from the localization procedure, and proposed their utilization as a post-VSCF correlation correction in the L-VSCF(HC) method.<sup>[47]</sup> Recently, Christiansen and co-workers proposed hybrid optimized/localized vibrational coordinates, where both the energy and spatial localization conditions are applied in the VSCF procedure.<sup>[48]</sup>

In this paper, we explore the use of localized modes in the L-VSCF/L-VCI framework for calculations of the full anharmonic vibrational spectra (i.e., of all fundamental vibrations) for small molecules. With these coordinates, we assess their benefits with respect to the main bottlenecks of such computations, the convergence of the  $n$ -mode expansion and the possibility to neglect its small contributions *a priori*, as well as the convergence of the VCI expansion with respect to the excitation space.

This work is organized as follows: First, we recall and introduce the main aspects of the theory, concerning the  $n$ -mode expansion (Section 2), the localization of normal modes (Section 3), and the L-VSCF and L-VCI methods (Section 4). Subsequently, the computational details are described in Section 5. Next, we apply these methods to perform anharmonic vibrational calculations for ethene in Section 6 and for furan in Section 7.

With high-level anharmonic potential energy surfaces for these two test cases, we investigate the mutual couplings of normal and localized modes, respectively (Sections 6.1 and 7.1), the convergence with respect to the VCI excitation space (Section 6.3) and the convergence of the  $n$ -mode expansion (Sections 6.2, 6.4, and 7.2). Our best-estimate (L-)VCI fundamental energies are compared to experimental reference data (Sections 6.4 and 7.2). At this point, we also explore simplified models to reduce the computational cost without a significant loss of accuracy. Finally, our conclusions are summarized in Section 8.

## 2 $n$ -mode expansion of the PES

The potential energy surface in our calculations is approximated by the hierarchical  $n$ -mode expansion,<sup>[8,9]</sup> i.e.,

$$\begin{aligned}
 V(\mathbf{q}) = & \sum_i^M V_i^{(1)}(q_i) + \sum_{i<j}^M V_{ij}^{(2)}(q_i, q_j) \\
 & + \sum_{i<j<k}^M V_{ijk}^{(3)}(q_i, q_j, q_k) + \sum_{i<j<k<l}^M V_{ijkl}^{(4)}(q_i, q_j, q_k, q_l) + \dots,
 \end{aligned} \tag{1}$$

with  $\mathbf{q}$  being  $M$  rectilinear coordinates,

$$q_i = \sum_{I=1}^{N_{\text{nuc}}} \sum_{\alpha=x,y,z} Q_{I\alpha}^i R_{I\alpha}^{(m)}, \tag{2}$$

where  $R_{I\alpha}^{(m)}$  is the mass-weighted Cartesian  $\alpha$ -coordinate ( $\alpha = x, y, z$ ) of nucleus  $I$  and where

$$\sum_{I\alpha} Q_{I\alpha}^i Q_{I\alpha}^j = \delta_{ij}. \tag{3}$$

The coefficients  $Q_{I\alpha}^i$  can be chosen as the normal-mode vectors obtained in the harmonic approximation, or as localized modes  $\tilde{Q}_{I\alpha}^i$  obtained via a transformation of the normal modes. Here and in the following the tilde denotes quantities referring to localized modes. Details will be discussed in Section 3.

To make the calculation of the PES feasible, the  $n$ -mode expansion is truncated at a certain order. It should be stressed that the PES in a truncated  $n$ -mode expansion is not invariant upon transformation of the modes, and thus the PES in localized-mode coordinates is not equivalent to the PES in normal-mode coordinates. Therefore, the PES in different coordinates have to be constructed separately. Consequently, the vibrational frequencies obtained with a truncated  $n$ -mode expansion in normal-mode coordinates and in localized-mode coordinates, respectively, will not be identical. This difference will, however, vanish when the  $n$ -mode expansion is fully converged. In contrast, a truncated Taylor expansion of the PES can be easily transformed to a representation in other rectilinear modes (for details, see Appendix A of Ref<sup>[36]</sup>).

### 3 Localization of normal modes

Here we recall only the crucial aspects of the method of normal modes localization, for further details see Ref.<sup>[39]</sup> We begin with the normal modes  $\mathbf{Q}$  obtained as eigenvectors of the mass-weighted molecular Hessian  $\mathbf{H}^{(m)}$ ,

$$\mathbf{H}^{(q)} = \mathbf{Q}^T \mathbf{H}^{(m)} \mathbf{Q}, \quad (4)$$

with corresponding eigenvalues (i.e., squared vibrational frequencies)  $H_{ii}^{(q)} = \omega_i^2 = 4\pi\nu_i^2$ . The corresponding normal-mode coordinates are then defined by Eq. 2. To arrive at



localized modes, the normal modes are transformed with a unitary transformation  $\mathbf{U}$ ,

$$\tilde{\mathbf{Q}} = \mathbf{Q}\mathbf{U}, \quad (5)$$

such that  $\mathbf{U}$  maximizes the localization measure  $\xi(\tilde{\mathbf{Q}})$ . Here, we apply the atomic-contribution criterion defined as<sup>[39]</sup>

$$\xi_{\text{at}}(\tilde{\mathbf{Q}}) = \sum_{p=1} \sum_{i=1} (\tilde{C}_{ip})^2, \quad (6)$$

where  $\tilde{C}_{ip}$  corresponds to the contribution of nucleus  $i$  to the normal mode  $\mathbf{Q}_p$  defined as

$$\tilde{C}_{ip} = \sum_{\alpha=x,y,z} (\tilde{Q}_{i\alpha,p})^2. \quad (7)$$

When localizing the normal modes, the Hessian in the basis of the localized modes,

$$\tilde{\mathbf{H}} = \mathbf{U}^T \mathbf{H}^{(q)} \mathbf{U}, \quad (8)$$

is no longer diagonal and the localized modes are not the eigenvectors of the molecular Hessian.

Commonly, the localization of the normal modes is performed for subsets of normal modes. To this end, the matrix  $\mathbf{Q}$  is divided into column vectors which are assigned to  $n_s$  subsets such that

$$\mathbf{Q} = \mathbf{Q}^{\text{sub},1} || \mathbf{Q}^{\text{sub},2} || \dots || \mathbf{Q}^{\text{sub},n_s}. \quad (9)$$

This leads to  $n_s$  distinct subsets of localized modes  $\{\tilde{\mathbf{Q}}^{\text{sub},i}\}$ . The resulting Hessian in the basis of these subset-localized modes is a block-diagonal matrix, containing a non-zero block  $\tilde{\mathbf{H}}^{\text{sub},i}$  for each subset of localized modes along its diagonal.

Different strategies can be used for assigning normal modes to subset in the localization procedure. The character of normal modes (i.e., bending, stretching etc.) can be used to decide which modes should be localized together. Furthermore, the frequencies of normal modes can be taken into account, and thus modes lying in a given region of the spectrum are grouped and localized together. Previously,<sup>[39–43]</sup> such criteria have been used to guide a normal mode assignment. We employ such criteria here for localizing the normal modes in subsets containing similar vibrations.

## 4 L-VSCF and L-VCI

We are aiming to solve the vibrational Schrödinger equation with the Watson Hamiltonian for a non-rotating molecule,<sup>[49]</sup>

$$\hat{H} = \frac{1}{2} \sum_{\alpha\beta} \hat{\pi}_\alpha \mu_{\alpha\beta} \hat{\pi}_\beta - \frac{1}{8} \sum_{\alpha} \mu_{\alpha\alpha} - \frac{1}{2} \sum_i^M \frac{\partial^2}{\partial q_i^2} + V(\mathbf{q}), \quad (10)$$

where the first term corresponds to the vibrational angular momentum (VAM), and the second is so-called Watson correction term, both together are often referred as VAM terms. Here,  $\boldsymbol{\mu}$  is the inverse moment of the inertia tensor, and  $\hat{\boldsymbol{\pi}}$  is the momentum operator. Since the exact evaluation of the VAM terms is cumbersome several approximations are commonly introduced, such as a hierarchical expansion of the  $\boldsymbol{\mu}$  tensor, or a selective inclusion of the terms in the VCI calculations in combination with prescreening techniques.<sup>[9,50]</sup> As the VAM terms depend on the inverse of the inertia tensor, their contribution will decrease with increasing size of the molecule. Thus, for simplicity and efficiency, they are often omitted entirely, as we proceed here,

$$\hat{H} = -\frac{1}{2} \sum_i^M \frac{\partial^2}{\partial q_i^2} + V(\mathbf{q}), \quad (11)$$

where  $V(\mathbf{q})$  is expressed as a truncated  $n$ -mode expansion in either the normal-mode coordinates  $\mathbf{q}$  or localized-mode coordinates  $\tilde{\mathbf{q}}$ .

For the approximate solution of the vibrational Schrödinger equation, the VSCF and VCI methods in normal-mode coordinates are well established.<sup>[6,7]</sup> Recently, we have introduced the analogous localized-mode variants L-VSCF and L-VCI.<sup>[45]</sup> Here, we briefly recall the essential steps.

The vibrational wavefunction in L-VSCF is given by the product ansatz,

$$\Psi_n(\tilde{\mathbf{q}}) \approx \psi_n(\tilde{q}_1, \dots, \tilde{q}_M) = \prod_i^M \phi_i^{n_i}(\tilde{q}_i). \quad (12)$$

Here,  $\phi_i^{n_i}(\tilde{q}_i)$  is a so-called modal for the  $i$ -th localized mode  $\tilde{q}_i$  and  $n_i$  is the vibrational quantum number for this modal. Applying the variational principle to the nuclear Schrödinger equation, a set of one-mode equations is obtained,

$$\hat{h}_i^n(\tilde{q}_i) \phi_i^{n_i}(\tilde{q}_i) = \epsilon_i^{n_i} \phi_i^{n_i}(\tilde{q}_i), \quad (13)$$

with the effective Hamiltonian,

$$\hat{h}_i^n(\tilde{q}_i) = -\frac{1}{2} \frac{\partial^2}{\partial \tilde{q}_i^2} + V_i^{(1)}(\tilde{q}_i) + V_i^n(\tilde{q}_i), \quad (14)$$

containing an effective mean-field potential,

$$\begin{aligned} V_i^n(\tilde{q}_i) = & \sum_j^M \langle \phi_j^{n_j} | V_{ij}^{(2)} | \phi_j^{n_j} \rangle + \sum_{j < k}^M \langle \phi_j^{n_j} \phi_k^{n_k} | V_{ijk}^{(3)} | \phi_j^{n_j} \phi_k^{n_k} \rangle \\ & + \sum_{j < k < l}^M \langle \phi_j^{n_j} \phi_k^{n_k} \phi_l^{n_l} | V_{ijkl}^{(4)} | \phi_j^{n_j} \phi_k^{n_k} \phi_l^{n_l} \rangle + \dots \end{aligned} \quad (15)$$

The resulting eigenvalue equations are then solved in a self-consistent manner to obtain the modal energies  $\epsilon_i^{n_i}$  as well as the optimized modals  $\phi_i^{n_i}(\tilde{q}_i)$  themselves.

The correlation energy is then treated using (L-)VCI.<sup>[17]</sup> In this method, a total wavefunction for a considered vibrational state is built as a linear combination of  $N_{\text{states}}$  L-VCI basis states,

$$\Psi_i^{\text{L-VCI}}(\tilde{\mathbf{q}}) = \sum_I^{N_{\text{states}}} c_I^{(i)} \psi_{\mathbf{n}_I}^0(\tilde{\mathbf{q}}) \quad (16)$$

The functions  $\psi_{\mathbf{n}_I}^0$  are products of the ground-state optimized L-VSCF modals  $\phi_i^{n_i,0}$ . Applying the variational principle with the ansatz of Eq. (16) leads to a CI eigenvalue equation with the CI-matrix,

$$\begin{aligned} \langle \psi_{\mathbf{n}_I}^0 | \hat{H} | \psi_{\mathbf{n}_J}^0 \rangle &= \sum_i^M \left\langle \phi_i^{n_I,0} \left| -\frac{1}{2} \frac{\partial^2}{\partial \tilde{q}_i^2} + V_i^{(1)} \right| \phi_i^{n_J,0} \right\rangle \prod_{j \neq i}^M \delta_{n_j^I n_j^J} \\ &+ \sum_{i < j}^M \left\langle \phi_i^{n_I,0} \phi_j^{n_I,0} \left| V_{ij}^{(2)} \right| \phi_i^{n_J,0} \phi_j^{n_J,0} \right\rangle \prod_{k \neq i,j}^M \delta_{n_k^I n_k^J} \\ &+ \sum_{i < j < k}^M \left\langle \phi_i^{n_I,0} \phi_j^{n_I,0} \phi_k^{n_I,0} \left| V_{ijk}^{(3)} \right| \phi_i^{n_J,0} \phi_j^{n_J,0} \phi_k^{n_J,0} \right\rangle \prod_{l \neq i,j,k}^M \delta_{n_l^I n_l^J} \\ &+ \sum_{i < j < k < l}^M \left\langle \phi_i^{n_I,0} \phi_j^{n_I,0} \phi_k^{n_I,0} \phi_l^{n_I,0} \left| V_{ijkl}^{(4)} \right| \phi_i^{n_J,0} \phi_j^{n_J,0} \phi_k^{n_J,0} \phi_l^{n_J,0} \right\rangle \prod_{m \neq i,j,k,l}^M \delta_{n_m^I n_m^J} \\ &+ \dots \end{aligned} \quad (17)$$

Its eigenvalues and eigenvectors are the requested L-VCI energies and L-VCI wavefunction coefficients, respectively. The CI expansion in Eq. (16) is limited to a given order of excitation. The inclusion of higher excitations leads towards the limit of the full VCI (FVCI), where all possible excitations are considered, but simultaneously increases the computational effort to construct and diagonalize the CI-matrix.

There are several ways of constructing the excitation space in VCI calculations. Christiansen proposed the most straightforward definition, denoted as VCI[ $n$ ], where for each of the  $M$  modals, excitations up to the  $n$ -th excited state are allowed.<sup>[51]</sup> Such a defini-

tion yields a rather large excitation space, and thus further limitations are introduced. Rauhut defines the number of simultaneously excited modals by analogy to electronic structure calculations giving VCI-S, VCI-SD, VCI-SDT,  $\dots$ , where up to one, two, and three modals are excited, respectively.<sup>[18]</sup> Additionally, two parameters  $n_{\max}^1$  and  $n_{\max}^{\Sigma}$  can be defined, limiting the maximal excitation per modal and the total sum of excitation quanta, respectively. Here, we equate the three parameters introduced by Rauhut. Thus, in our nomenclature VCI-SDTQ corresponds to a VCI space where up to four mode are excited simultaneously with up to four excitation quanta,  $n_{\max}^1 = n_{\max}^{\Sigma} = 4$ . Yagi *et al.* reported that such a definition, denoted by them as VCI- $(k)$ , is rational for VCI in the basis of optimized modals.<sup>[36]</sup>

In our calculations, the excitation space is constructed from a single VSCF reference, which was optimized for the vibrational ground state. This approach is referred to as ground-state VCI (gs-VCI). Another possibility is to use a different VSCF reference for each state of interest, which was optimized in this particular state, denoted state-specific VCI (ss-VCI). Such calculations should usually provide a faster convergence with respect to the excitation space.<sup>[52]</sup> However, it requires more computational effort, and yields non-orthogonal VCI wave functions.

## 5 Computational details

For ethene and furan we have used the normal modes, harmonic frequencies and anharmonic potential energy surfaces in terms of normal-mode coordinates available in the online Database of Potential Energy Surfaces maintained by Rauhut and co-workers.<sup>[1,12,53]</sup> These harmonic and anharmonic potential energy surfaces were constructed by means of highly accurate explicitly correlated CCSD(T)-F12x methods.<sup>[1]</sup> Namely, the CCSD(T)-F12b method with a cc-pVTZ-F12 basis set was used to obtain the Hessian and the

anharmonic one-mode potentials, whereas CCSD(T)-F12a with a cc-pVDZ-F12 basis set was used for the anharmonic two-mode and higher-order potentials.<sup>[54–56]</sup> For constructing anharmonic potential energy surfaces in terms of localized modes, we have localized the CCSD(T)-F12b/cc-pVTZ-F12 normal modes using our LocVib package.<sup>[39,57]</sup> Subsequently, we used the same methods as Rauhut and co-workers to calculate the one-mode as well as (for ethene) the two-mode and three-mode potentials in terms of localized-mode coordinates with the MOLPRO 2012.1 program package.<sup>[58]</sup>

To investigate the VCI convergence with respect to the  $n$ -mode expansion of the PES for the four highest modes of ethene (see Section 6.2), both for normal and localized modes, up to four-mode anharmonic potentials were obtained using density-functional theory (DFT) with the TURBOMOLE 6.3.1 program package.<sup>[59,60]</sup> The BP86 exchange–correlation functional<sup>[61,62]</sup> with Ahlrichs’ def2-TZVP basis sets<sup>[63]</sup> in combination with the resolution-of-identity (RI) approximation and suitable auxiliary basis set was used.<sup>[64,65]</sup>

Additionally, for furan we have constructed so-called hybrid potential energy surfaces, where the lower-order surfaces have been calculated with higher accuracy, whereas the higher-order surfaces have been calculated with lower accuracy.<sup>[12,16]</sup> We use a hybrid PES in terms of both normal-mode and localized-mode coordinates. Here, CCSD(T)/F12b is used to calculate the one-mode potentials, while the two-mode potentials are obtained with DFT (BP/def2-TZVP) as described above. Further details are discussed in Section 7.2.

(L-)VSCF/(L-)VCI calculations were carried out with our Python code VIBRATIONS.<sup>[45]</sup> All calculations were performed on equally spaced 16-point grids (see Ref.<sup>[45]</sup> for further details). VIBRATIONS allows to perform VSCF and VCI calculations with user-defined vibrational coordinates. The calculations can be carried out for all vibrational modes, as well as for a chosen subset of those. For constructing potential energy surfaces, our code uses PyADF<sup>[66]</sup> as an interface to various quantum-chemistry packages. VCI calcula-

tions are performed in the basis of ground-state optimized VSCF wave function, within a freely defined excitation space. Large Hamiltonian matrices can be efficiently constructed using parallel techniques, distributing the work over many cores, whereas the diagonalization can be effectively performed in an iterative manner, utilizing tools available in the SCIPY<sup>[67]</sup> and NUMPY<sup>[68]</sup> packages.

## 6 Test case: ethene

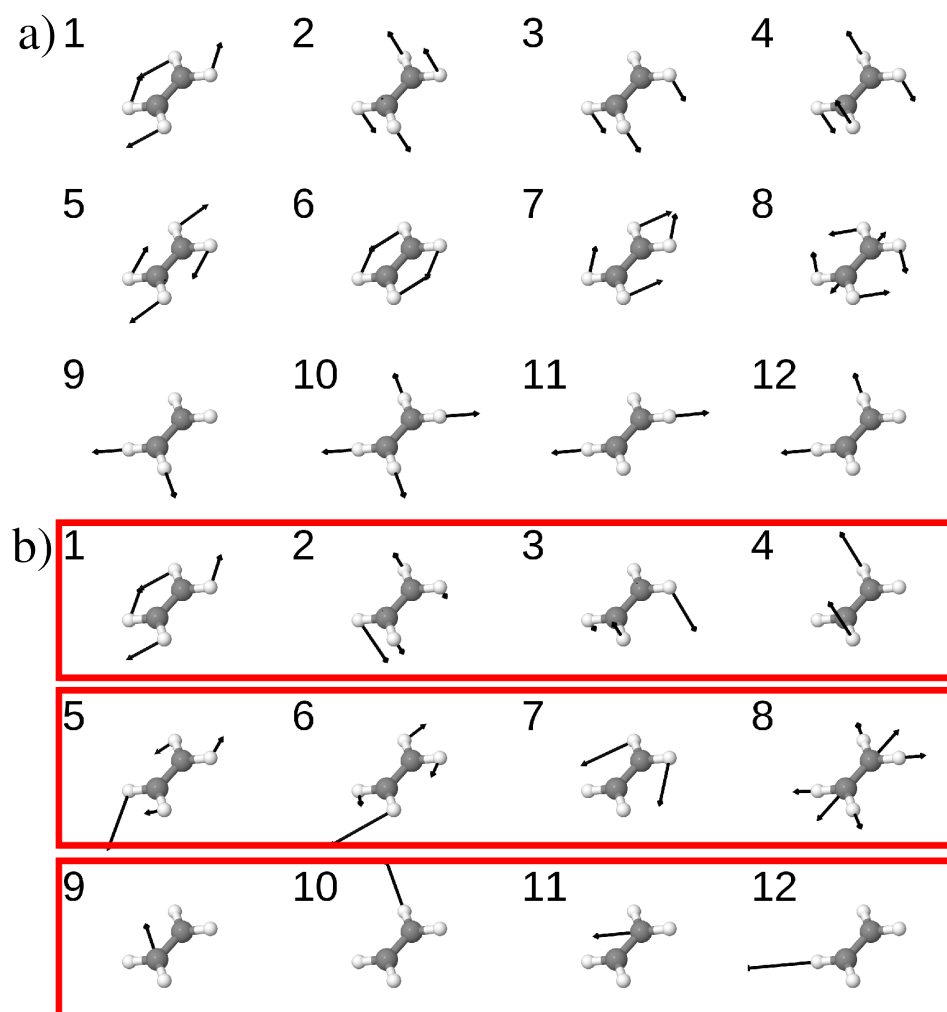
To explore the advantages of L-VSCF/L-VCI over a conventional VSCF/VCI treatment, we consider the ethene molecule as a first test case. Ethene has been extensively used in benchmarks of different methods for calculating anharmonic vibrational frequencies, and therefore rich reference data are available.<sup>[1, 4, 52, 69, 70]</sup>

### 6.1 Normal and localized modes

Graphical representations of the normal modes of the ethene molecule are shown in Fig. 1a, and the corresponding harmonic vibrational frequencies are listed in Table I. The first eight modes correspond to in-plane and out-of-plane bending vibrations, while the final four are C–H stretching modes. For the localization, we have assigned the normal modes to three subsets, each consisting of four modes corresponding to characteristic groups of vibrations. This assignment as well as the resulting localized modes are presented in Fig. 1b. Visually, the main character of the first eight modes is essentially unchanged upon localization, but in many cases there is a more distinct contribution of one single vibration. On the other hand, the collective C–H stretching vibrations are decomposed into four distinct single-bond C–H stretching vibrations by the localization.

The fictitious vibrational frequencies of the localized modes (see Table I) are on average

Figure 1: (a) Normal and (b) localized modes for ethene (CCSD(T)-F12b/cc-pVTZ-F12). The localization was carried out in the three subsets also indicated here.



$39 \text{ cm}^{-1}$  off from the harmonic frequencies. However, a L-VCI-S calculation using the harmonic PES expressed in localized-mode coordinates recovers the original harmonic frequencies within at most  $2 \text{ cm}^{-1}$ .

Before turning to the full anharmonic calculations for ethene, we investigate how the choice of normal-mode coordinates or localized-mode coordinates affects the coupling between the modes via the two-mode potentials. To this end, the magnitude of the coupling between modes  $i$  and  $j$  is calculated as the absolute value of the expectation value of the



Table I: Normal-mode ( $\nu$ ) and localized-mode ( $\tilde{\nu}$ ) vibrational frequencies for ethene (CCSD(T)-F12b/cc-pVTZ-F12). The results of L-VCI-S using the harmonic PES expressed in localized-mode coordinates are also included, along with the mean average deviation (MAD) and their maximum absolute deviation (MAX) from the normal-mode harmonic frequencies. All frequencies are given in  $\text{cm}^{-1}$ .

Mode	Normal	Localized Modes			
	$\nu$	$\tilde{\nu}$		L-VCI-S	
1	825	825	0	825	0
2	949	977	28	949	-1
3	963	977	14	963	0
4	1050	1008	-42	1051	1
5	1248	1354	106	1246	-2
6	1368	1354	-15	1369	1
7	1477	1462	-15	1476	-2
8	1671	1595	-76	1673	2
9	3140	3191	51	3140	0
10	3155	3191	36	3155	0
11	3222	3191	-31	3222	0
12	3248	3191	-57	3248	0
MAD			39		1
MAX			106		2

two-mode potential operator for modes  $i$  and  $j$  with the ground-state optimized VSCF wave function [cf. Eq. (15)],

$$C(i, j) = \left| \left\langle \phi_i^{0,0} \phi_j^{0,0} \left| V_{ij}^{(2)} \right| \phi_i^{0,0} \phi_j^{0,0} \right\rangle \right|, \quad (18)$$

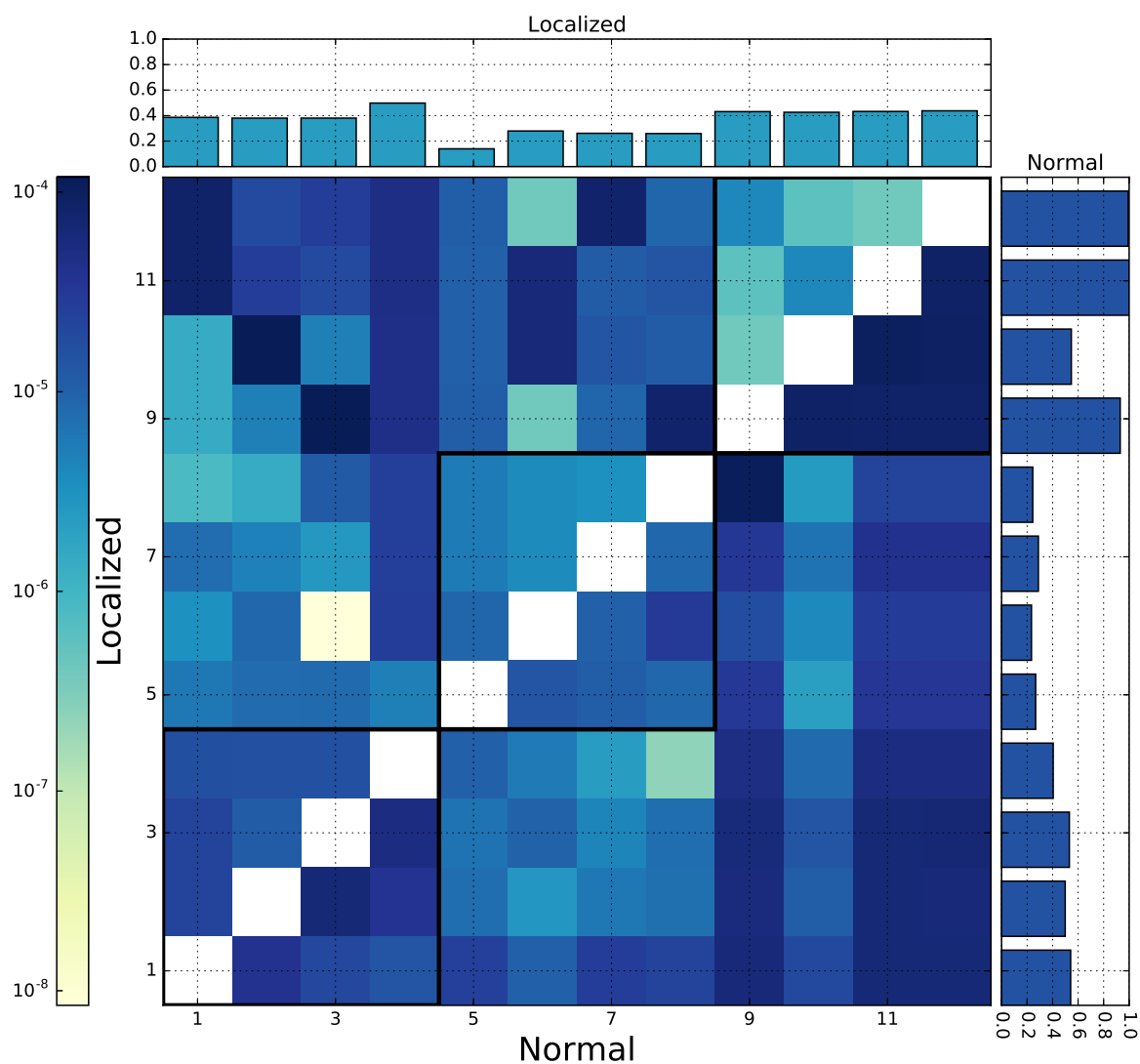
where  $\phi_i^{0,0}$  is the ground-state optimized VSCF modal for the  $i$ -th mode in its ground-state.

These couplings are visualized in Fig. 2. Here, the upper triangle of the matrix corresponds to the localized modes, whereas the lower triangle corresponds to the normal modes. The black boxes indicate modes that were localized together. Noticeably, the coupling between the localized modes within subsets is smaller than for the corresponding normal modes, which is especially pronounced for the C–H stretching modes (modes 9–12). The bar charts present the total coupling of the  $i$ -th normal or localized mode with other modes, calculated as  $C(i) = \sum_{j \neq i} C(i, j)$ . For these total couplings of C–H stretching vibrations, one can notice that the localized modes are not only less coupled within their subsets, but that they are also less coupled with all other modes. Overall, the localized modes show weaker couplings, with some stronger individual spots, whereas the normal modes have rather uniformly strong couplings. Thus, already for a molecule as small as ethene, switching from normal modes to localized modes can reduce the two-mode couplings. These benefits can be expected to become larger as the size of the considered molecule increases,<sup>[45]</sup> especially for the lower-frequency modes.

## 6.2 Convergence of the $n$ -mode expansion: C–H stretching modes

To analyze the convergence of (L-)VCI calculations with respect to the order of the  $n$ -mode expansion, we initially consider only one subset of normal modes, namely the four C–H stretching vibrations. In this subset, for both normal and localized modes, all potentials

Figure 2: Strengths of the two-mode couplings,  $C(i, j)$ , for the normal and localized modes (central figure) and total coupling of the  $i$ -th normal and localized mode with all other modes (bar plots),  $C(i)$ , for ethene. The lower right part refers to normal modes, whereas the upper left part refers to localized modes. See text for further details.



up to the fourth order were calculated by means of density-functional theory (DFT), using grids with 16 points along each mode. The construction of this approximated PES required 83 520 single-point calculations in total (64, 1 536, 16 384, and 65 536, for  $V^{(1)}$ ,  $V^{(2)}$ ,  $V^{(3)}$ , and  $V^{(4)}$ , respectively). These potentials were employed in VCI and L-VCI calculations, and up to quintuple excitations were considered [(L-)VCI-SDTQ5]. The results are shown in Table II.

If the  $n$ -mode expansion is performed in terms of normal-mode coordinates, it is clear that up to four-mode potentials need to be included. Neglecting the four-mode potentials and including only the contributions up to  $V^{(3)}$  leads to deviations of up to  $20 \text{ cm}^{-1}$  in the resulting vibrational frequencies. This changes if the PES expanded in terms of localized-mode coordinates. In this case, already L-VCI with only one-mode and two-mode potentials yields converged results, with deviations of at most  $1 \text{ cm}^{-1}$  from the normal-modes reference. A significant difference can be observed in the VCI expansions for both cases. For the normal modes, each of the converged C–H transitions consists to at least 95% of the respective singly-excited VSCF state. In the localized-mode basis, these transitions are combinations of the four singly excited L-VSCF states with roughly equal weights. Furthermore, it is remarkable that already L-VCI-S (i.e., including only single excitations) gave vibrational frequencies being within  $4 \text{ cm}^{-1}$  agreement with the values presented in the table. Thus, when using localized-mode coordinates instead of normal-mode coordinates, only 1600 single-point calculations (instead of 83 520 single-point calculations) and a significantly smaller excitation space (VCI-S instead of VCI-SDTQ5) are necessary to reach the same accuracy. Note that these one-mode potentials in localized-mode coordinates are transformed into up to four-mode potentials when going to normal modes because each localized modes is a linear combination of four normal modes.

Table II: Convergence of the (L-)VCI-SDTQ5 fundamental vibrational frequencies for the C–H stretching vibrations in ethene (DFT/BP/def2-TZVP) with respect to the order of the  $n$ -mode expansion.  $V^{\{n\}}$  denotes the orders of the potentials included in the respective calculations. Only the subset of the C–H stretching vibrations is considered here and all couplings to other modes are neglected. For the frequencies obtained with up to two- and three-mode potentials, the deviations, mean absolute deviations (MAD), and maximal absolute deviations (MAX) with respect to the results including up to four-mode potentials are also included. All frequencies are given in  $\text{cm}^{-1}$ .

Mode	Normal Modes			Localized Modes		
	$V^{(1,2)}$	$V^{(1,2,3)}$	$V^{(1,2,3,4)}$	$V^{(1,2)}$	$V^{(1,2,3)}$	$V^{(1,2,3,4)}$
9	2969 19	2930 -20	2950	2949 0	2949 0	2949
10	3010 49	2954 -7	2961	2960 1	2961 0	2961
11	3073 62	2991 -20	3011	3010 0	3010 0	3010
12	3104 63	3020 -21	3041	3040 0	3040 0	3040
MAD	48	17		0	0	
MAX	63	21		1	0	

### 6.3 Convergence of the VCI expansion

Next, we consider all modes and investigate the convergence of the fundamental frequencies with respect to the excitation space used in the (L-)VCI Hamiltonian. Here, the PES was approximated by the  $n$ -mode expansion in terms of normal-mode coordinates or localized-mode coordinates, truncated after two-mode or three-mode potentials. For both the expansion in normal-mode coordinates and in localized-mode coordinates, the fundamental frequencies obtained at each VCI excitation level as well as their deviations from the reference values obtained at the (L-)VCI-SDTQ56 level are listed in Tables III and IV, respectively.

Looking at the results in normal-mode coordinates (cf. Table III), the calculations with up to two-mode potentials are converged within  $1 \text{ cm}^{-1}$  when quintuple excitation are included. The initial VCI-S fundamentals are on average  $25 \text{ cm}^{-1}$  off from the reference,

Table III: Convergence of the VCI-SDTQ5 fundamental vibrational frequencies of ethene (CCSD(T)-F12x) with respect to the order of the VCI expansion. In each column, the vibrational frequencies are given together with their deviations from the VCI-SDTQ56 value as well as the mean average deviation (MAD) and their maximum absolute deviation (MAX). The calculations have been performed for different truncations of the  $n$ -mode expansion in terms of normal-mode coordinates.  $V^{\{n\}}$  denotes the orders of the potentials included in the respective calculations. All frequencies are given in  $\text{cm}^{-1}$ .

Normal Modes, $V^{(1,2)}$											
Mode	VCI-S		-SD		-SDT		-SDTQ		-SDTQ5		-SDTQ56
1	847	16	839	8	867	37	834	4	830	0	830
2	951	11	946	6	974	34	943	3	940	0	940
3	966	13	959	7	988	35	956	3	952	0	952
4	1037	8	1033	4	1062	33	1031	3	1029	0	1029
5	1235	3	1233	2	1262	31	1233	2	1231	0	1231
6	1350	8	1345	3	1374	32	1344	2	1342	0	1342
7	1450	3	1449	2	1478	31	1449	2	1447	0	1447
8	1642	15	1633	6	1661	34	1632	5	1627	1	1627
9	3058	54	3021	17	3049	45	3010	6	3005	0	3004
10	3059	52	3033	26	3061	53	3015	7	3008	0	3008
11	3131	59	3087	16	3114	43	3074	3	3071	0	3071
12	3157	58	3114	16	3141	43	3101	3	3099	0	3098
MAD	25		9		38		4		0		
MAX	59		26		53		7		1		
Normal Modes, $V^{(1,2,3)}$											
1	850	28	832	11	895	73	825	4	821	-1	821
2	955	26	938	9	1001	72	933	3	929	-1	929
3	970	29	952	10	1014	73	945	4	941	-1	942
4	1041	23	1026	8	1089	71	1021	3	1017	-1	1018
5	1237	14	1227	4	1291	67	1225	2	1222	-1	1223
6	1352	11	1344	3	1407	66	1344	2	1340	-1	1341
7	1454	17	1442	5	1505	68	1440	3	1437	-1	1437
8	1644	21	1630	8	1692	70	1629	7	1622	0	1622
9	3060	106	3004	51	3059	106	2975	22	2955	2	2953
10	3067	71	3043	46	3096	99	3016	19	3001	4	2997
11	3140	93	3106	59	3160	113	3070	23	3050	3	3047
12	3166	100	3126	60	3180	114	3085	18	3069	2	3066
MAD	45		23		83		9		1		
MAX	106		60		114		23		4		

Table IV: Convergence of the L-VCI-SDTQ5 fundamental vibrational frequencies of ethene (CCSD(T)-F12x) with respect to the order of the VCI expansion. In each column, the vibrational frequencies are given together with their deviations from the L-VCI-SDTQ56 value as well as the mean average deviation (MAD) and their maximum absolute deviation (MAX). The calculations have been performed for different truncations of the  $n$ -mode expansion in terms of localized-mode coordinates.  $V^{\{n\}}$  denotes the orders of the potentials included in the respective calculations. All frequencies are given in  $\text{cm}^{-1}$ .

Mode	L-VCI-S		-SD		-SDT		-SDTQ		-SDTQ5		-SDTQ56
Localized Modes, $V^{(1,2)}$											
1	839	21	843	24	845	26	826	8	820	2	818
2	938	25	940	27	940	28	922	9	915	2	913
3	967	23	969	25	971	26	953	8	946	2	944
4	1039	24	1040	26	1039	25	1022	8	1016	2	1014
5	1226	12	1236	22	1234	20	1220	6	1215	1	1214
6	1342	14	1351	23	1347	19	1334	6	1329	1	1328
7	1458	10	1467	19	1466	18	1453	5	1449	1	1448
8	1653	25	1659	31	1653	25	1641	13	1633	5	1628
9	2961	-10	2985	14	2988	17	2973	2	2974	3	2971
10	2976	-40	3039	22	3040	24	3024	8	3017	0	3017
11	3045	-11	3072	17	3074	19	3062	6	3057	1	3055
12	3072	-9	3099	17	3101	19	3088	6	3082	1	3081
MAD	19		22		22		7		2		
MAX	40		31		28		13		5		
Localized Modes, $V^{(1,2,3)}$											
1	850	33	845	27	855	38	830	12	820	3	817
2	951	31	948	27	958	38	933	12	923	3	920
3	970	30	966	26	977	36	952	12	943	3	940
4	1043	25	1041	23	1050	33	1028	10	1020	2	1017
5	1240	20	1243	23	1251	31	1229	9	1222	2	1220
6	1355	13	1361	18	1369	26	1351	8	1345	2	1343
7	1454	20	1454	20	1464	30	1443	9	1436	2	1434
8	1645	26	1645	26	1650	31	1631	12	1622	4	1619
9	2974	-2	2996	20	3011	35	2991	14	2980	4	2976
10	2990	-23	3033	20	3045	32	3027	15	3018	5	3012
11	3039	-37	3095	19	3107	31	3089	13	3080	4	3076
12	3066	-32	3116	18	3128	29	3109	11	3101	2	3098
MAD	24		22		32		11		3		
MAX	37		27		38		15		5		

while the mean deviation decreases to only  $9 \text{ cm}^{-1}$  when including double excitations. However, when going to VCI-SDT there is a pronounced increase of the mean deviation to  $38 \text{ cm}^{-1}$ . In general, the convergence is faster for the low-frequency bending modes, whereas the C–H stretching modes converge significantly slower. A similar convergence pattern is observed for the calculations including up to three-mode potentials. Here, however, the deviations for each excitation level are roughly twice as high as for the PES including only two-mode potentials. Moreover, the VCI-SDTQ5 C–H stretching frequencies seem to be not fully converged, and an even larger excitation space might be needed to reach full convergence.

In localized-mode coordinates (cf. Table IV), the fundamental frequencies generally converge more smoothly. Already with L-VCI-S, the mean average deviation is smaller than when using normal-mode coordinates. Both for the calculations including up to two-mode and up to three-mode potentials, the deviations upon inclusion of triple excitations is smaller than in the normal modes case. Moreover, when going from the PES including only two-mode potentials to the one including also three-mode potentials, the increase of the mean average deviation is smaller than for the expansion of the potential energy surface in normal-mode coordinates. On the other hand, also in localized-mode coordinates, the L-VCI-SDTQ5 frequencies appear to be not fully converged.

## 6.4 Convergence of the $n$ -mode expansion for all fundamentals

In Table V, we compare the best-estimate results for VCI and L-VCI with different truncations of the  $n$ -mode expansion of the PES to the experimental reference values. Here, the VCI excitation space contains up to sextuple excitations both for normal and localized modes. For VCI, we use the PES approximated with up to the four-mode terms, whereas for L-VCI only up to the three-mode terms are included.



Table V: (L-)VCI-SDTQ56 fundamental vibrational frequencies calculated for ethene with different truncations of the  $n$ -mode expansion of the PES [CCSD(T)-F12x].  $V^{\{n\}}$  denotes the orders of the potentials included in the respective calculations,  $^{2h}$  refers to two-mode potentials obtained within the harmonic approximation. In each column, the frequencies are given together with their deviations from the experimental reference value as well as the mean average deviation (MAD) and their maximum absolute deviation (MAX). . All frequencies given in  $\text{cm}^{-1}$ .

Mode	Normal Modes								Localized Modes						Exp. <sup>a</sup>
	$V^{(1)}$		$V^{(1,2)}$		$V^{(1,2,3)}$		$V^{(1,2,3,4)}$		$V^{(1,2h)}$		$V^{(1,2)}$		$V^{(1,2,3)}$		
1	863	37	830	5	821	-5	819	-7	863	37	818	-8	817	-9	826
2	975	35	940	0	929	-11	927	-13	990	50	913	-27	920	-20	940
3	990	41	952	4	942	-7	939	-10	999	50	944	-4	940	-9	949
4	1062	36	1029	3	1018	-8	1016	-9	1083	57	1014	-11	1017	-8	1026
5	1253	31	1231	9	1223	1	1222	0	1257	35	1214	-8	1220	-2	1222
6	1370	27	1342	-2	1341	-2	1340	-3	1368	25	1328	-16	1343	-1	1344
7	1480	38	1447	5	1437	-5	1437	-6	1483	40	1448	6	1434	-8	1443
8	1668	42	1627	1	1622	-3	1621	-5	1661	35	1628	3	1619	-7	1625
9	3128	140	3004	16	2953	-35	2984	-4	3018	30	2971	-18	2976	-12	2989
10	3171	149	3008	-14	2997	-25	3019	-3	3033	11	3017	-5	3012	-10	3022
11	3258	174	3071	-12	3047	-36	3071	-13	3102	18	3055	-28	3076	-7	3083
12	3282	177	3098	-6	3066	-39	3094	-11	3128	23	3081	-24	3098	-7	3105
	MAD	77		6		15		7		34		13		8	
	MAX	177		16		39		13		57		28		20	

<sup>a</sup> – experimental values as referenced in Ref.<sup>[69]</sup>

Normal-mode VCI fundamental frequencies with the PES approximated with at most two-mode potentials have an MAD of  $6 \text{ cm}^{-1}$ . When going to a more accurate PES including also the three-mode terms, the mean average deviation increases to  $15 \text{ cm}^{-1}$ . Here, the C–H stretching modes contribute the most to this discrepancy. Inclusion of the four-mode terms in the  $n$ -mode expansion reduces the MAD to  $7 \text{ cm}^{-1}$ , predominantly for the C–H stretching modes.

Local-mode L-VCI with one-mode and two-mode potentials included delivers fundamental transition which are on average  $13 \text{ cm}^{-1}$  off from the reference. This is a deviation of similar magnitude as for the normal-modes VCI with up to three-mode potential included. However, the problematic C–H stretching modes energies are slightly better reproduced in the L-VCI case. Inclusion of the three-mode potentials in the PES expansion reduces the MAD to  $8 \text{ cm}^{-1}$ , which in turn is similar to the MAD of normal-modes VCI including up to four-mode potentials. This resembles the previously observed faster convergence with respect to the order of the  $n$ -mode expansion for the subset of C–H stretching modes (cf. Table II).

Despite the use of highly accurate potential energy surfaces with up to four or three-mode potentials included, there is still some deviation with respect to the experimental reference values. This is most likely due to the use of the simplified vibrational Hamiltonian given in Eq. 11 (see also Table II in Ref.<sup>[1]</sup>). Additionally, a rather compact excitation space was used and it might be necessary to include even higher excitations in the VCI expansion.

Finally, we also explore a low-cost model that could serve a first approximation of anharmonic corrections. Since the Hessian in the localized modes basis is not diagonal, the arising off-diagonal elements can be used to calculate harmonic two-mode potentials.<sup>[45]</sup> These can be combined with the anharmonic one-mode potentials. This approximate PES is labelled  $V^{(1,2h)}$  in Table V. Strong discrepancies can be observed for the bending modes, with deviations of up to  $57 \text{ cm}^{-1}$ . However, the C–H stretching modes are reproduced

quite well and the overall MAD is  $34\text{ cm}^{-1}$ . If the PES is expanded in normal modes, with the same computational effort one can calculate only the anharmonic one-mode potentials,  $V^{(1)}$ . Here, the deviation for the bending modes is at a similar level, but the C–H stretching modes are at least  $140\text{ cm}^{-1}$  off from the experiment. Thus, using localized modes in such a low-cost model, we reduce the error by over  $130\text{ cm}^{-1}$  for the C–H stretching vibrations, while staying in a similar error range for the bending modes.

In summary, calculations performed for ethene with localized modes showed that these coordinates yield fundamental transition energies that are equivalent to those obtained with normal modes. However, with local modes a smaller expansion of the PES could be applied. In localized-mode coordinates, already a PES including up to three-mode potentials gives fundamental vibrational frequencies that are as accurate as those obtained with a PES expanded in normal-mode coordinates including up to four-mode potentials. Thus, the number of required single-point energy calculations can be reduced from 33 358 528 in the case of normal-mode coordinates to only 918 208 in the case of localized mode coordinates. Moreover, localized modes seem to be more suitable for devising low-cost models that can give a first estimate of anharmonic effects by including only one-mode potentials and harmonic two-mode potentials. Finally, the convergence of the VCI expansion is smoother when using localized-mode coordinates, and smaller deviations are observed at low excitation level, which can again be exploited for devising low-cost models.

## 7 Furan

Another test system for our method was furan. It is a small heterocyclic aromatic molecule, in which in addition to the C–H stretching vibrations also ring vibrations are present. This molecule has extensively been used to benchmark methods for anharmonic vibrational calculations.<sup>[1,71–75]</sup>

## 7.1 Normal and localized modes

The CCSD(T)-F12b/cc-pVTZ normal modes for furan are shown in Fig. 3a and the corresponding harmonic frequencies are listed in Table VI. For the localization, the normal modes have been assigned to subsets according to their character and their harmonic frequencies. These subsets as well as the resulting localized modes are shown in Fig. 3b, whereas the resulting fictitious harmonic frequencies of the localized modes are listed in Table VI.

The normal modes are rather delocalized over the entire molecule and each normal mode involves many atoms. After the localization, some of them remain unchanged, or at least are still delocalized. However, in some cases a localization is observed, namely for the subsets of modes 3–6, modes 9–14 and modes 18–21. In the first of these subsets (modes 3–6), each mode corresponds to different out-of-plane bending of the C–H group. The second of these subsets (modes 9–14), are single C–H in-plane bending vibrations, except for modes 11 and 12 involving the oxygen atom. The last one of these subsets (modes 18–21) consists of single C–H stretching vibrations. L-VCI-S calculations using the harmonic PES expanded in localized-mode coordinates reproduce the initial normal-mode harmonic frequencies within on average  $1 \text{ cm}^{-1}$ , with a maximal deviation of  $6 \text{ cm}^{-1}$  for mode 14 (see Table VI).

Also for furan, we compare the two-mode couplings in normal-mode coordinates and in localized-mode coordinates. These are visualized in Fig. 4. Similarly to the ethene case, in localized-mode coordinates the mutual couplings are weaker, which is especially pronounced for the C–H out-of-plane bending vibrations (modes 3–6), and for the C–H stretching vibrations (modes 18–21). This also shows up in the total couplings shown in the bar charts, which are visibly smaller for the localized modes of these subsets compared to corresponding normal modes. In general, the localized modes are weaker coupled, with some single strong couplings, whereas for the normal modes one finds rather uniformly

Figure 3: (a) Normal and (b) localized modes for furan (CCSD(T)-F12b/cc-pVTZ-F12). The localization was carried out in the subsets also indicated here.

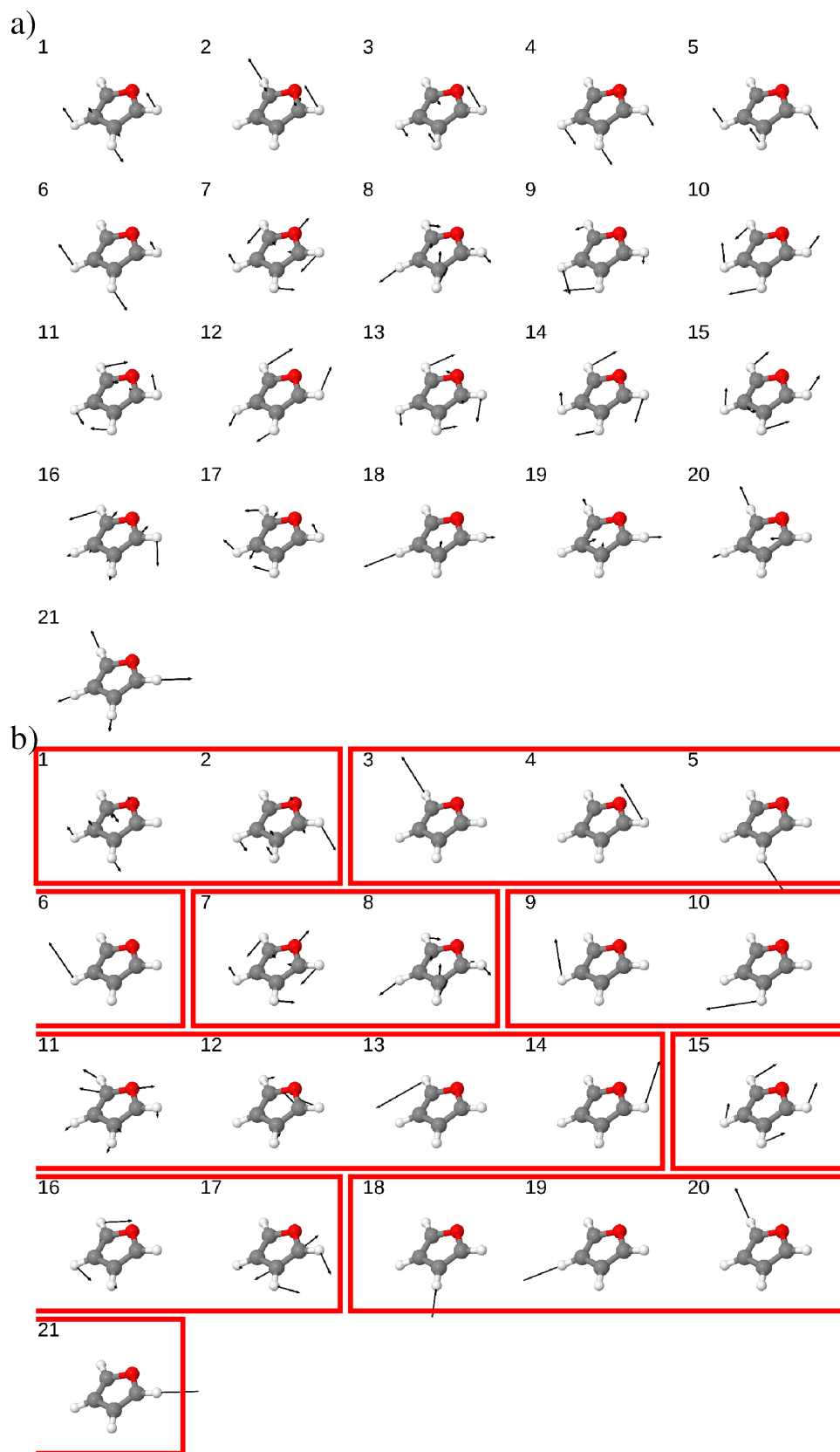


Table VI: Normal-mode ( $\nu$ ) and localized-mode ( $\tilde{\nu}$ ) vibrational frequencies for furan (CCSD(T)-F12b/cc-pVTZ-F12). The results of L-VCI-S using the harmonic PES expressed in localized-mode coordinates are also included, along with the mean average deviation (MAD) and their maximum absolute deviation (MAX) from the normal-mode harmonic frequencies. All frequencies are given in  $\text{cm}^{-1}$ .

No.	Normal	Localized Modes		
	$\nu$	$\tilde{\nu}$		L-VCI-S
1	607	610	3	607 0
2	614	610	-3	614 0
3	736	788	52	736 0
4	758	788	30	757 0
5	854	824	-30	853 0
6	876	824	-52	876 0
7	879	879	0	879 0
8	888	888	0	888 0
9	1012	1099	87	1012 0
10	1063	1099	35	1062 -2
11	1089	1135	46	1087 -2
12	1161	1135	-26	1158 -3
13	1218	1183	-34	1217 0
14	1291	1183	-108	1297 6
15	1418	1438	20	1419 0
16	1523	1548	25	1523 0
17	1593	1548	-45	1593 0
18	3255	3265	10	3255 0
19	3266	3265	-1	3265 0
20	3286	3284	-1	3286 0
21	3292	3284	-8	3292 0
		MAD	29	1
		MAX	108	6

strong couplings. This aspect is especially noticeable for the well-localized subsets of modes 3–6 and modes 18–21.

## 7.2 Convergence of the $n$ -mode expansion and hybrid PES

We have performed (L-)VCI-SDTQ5 calculations for different potential energy surfaces expanded in normal-mode coordinates and in localized-mode coordinates. These will be introduced in the following. The resulting fundamental vibrational frequencies are compared to the experimental results in Table VII.

When expanding the PES in normal-mode coordinates, VCI calculations with an accurate PES including up to three-mode potential, denoted  $V_{\text{CC}}^{(1,2,3)}$ , yield fundamental transitions that are on average  $6 \text{ cm}^{-1}$  off from the experiment. The largest deviations of up to  $27 \text{ cm}^{-1}$  are observed for the C–H stretching vibrations. To construct such a PES directly, neglecting symmetry and automated fitting procedures and assuming a 16-point grid for each mode, requires performing 336 CCSD(T)-F12b/cc-pVTZ-F12 single-point calculations for the one-mode potential, and in total 5 501 776 CCSD(T)-F12a/cc-pVDZ-F12 single-point calculations for the two- and three-mode terms.

For an approximation that is computationally less demanding, we have decided to use a hybrid PES, in which CCSD(T)-F12b/cc-pVTZ-F12 is used for the one-mode potentials, while DFT/BP/def2-TZVP calculations were employed for the two-mode terms and the three-mode potentials are neglected. This hybrid PES is denoted  $V_{\text{CC}}^{(1)} + V_{\text{DFT}}^{(2)}$ . If normal-mode coordinates are used, VCI-SDTQ5 calculations with such a PES give fundamental frequencies that deviate on average  $19 \text{ cm}^{-1}$  and at most  $66 \text{ cm}^{-1}$  from the reference values.

In contrast, if localized-mode coordinates are used, such calculations yield frequencies that are on average  $6 \text{ cm}^{-1}$  and at most  $15 \text{ cm}^{-1}$  off from the experimental results. Thus, the

Figure 4: Strengths of the two-mode couplings,  $C(i, j)$ , for the normal and localized modes (central figure) and total coupling of the  $i$ -th normal and localized mode with all other modes (bar plots),  $C(i)$ , for furan. The lower right part refers to normal modes, whereas the upper left part refers to localized modes. See Section 6.1 for further details.

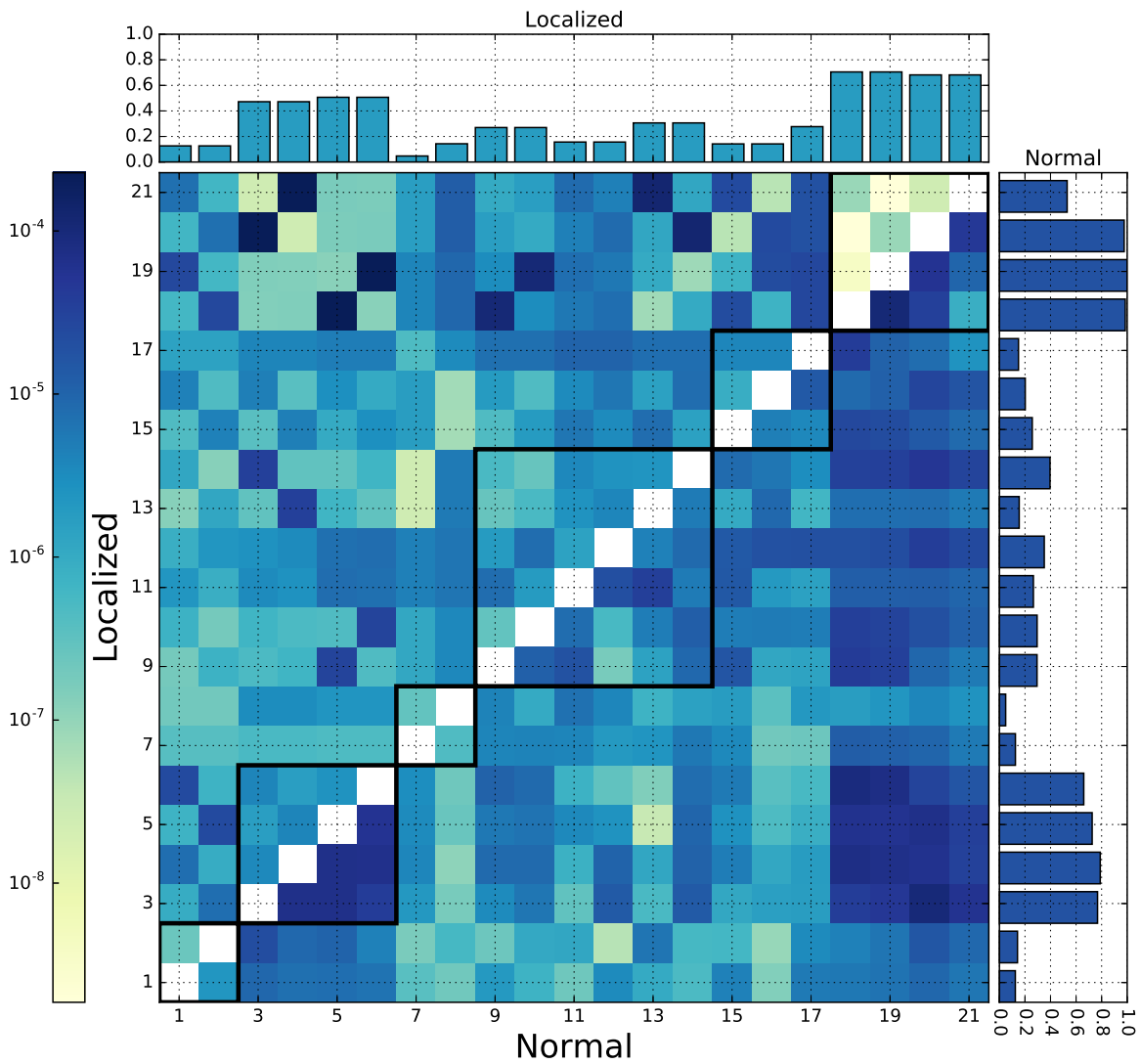




Table VII: (L-)VCI-SDTQ56 fundamental vibrational frequencies calculated for furan with different approximations for the PES (CC – contributions obtained with CCSD(T)-F12x, DFT – contributions obtained with DFT/BP/def2-TZVP;  $^{(n)}$  – order in the  $n$ -mode expansion,  $^{(2h)}$  – two-mode potentials obtained within the harmonic approximation,  $^{(2s)}$  – two-mode potentials in which the contributions of modes belonging to the same subset have been removed; See text for details). In each column, the frequencies are given together with their deviations from the experimental reference value as well as the mean average deviation (MAD) and their maximum absolute deviation (MAX). All frequencies given in  $\text{cm}^{-1}$ .

No.	Normal Modes						Localized Modes						Exp. <sup>a</sup>
	$V_{\text{CC}}^{(1)}$		$V_{\text{CC}}^{(1)} + V_{\text{DFT}}^{(2)}$		$V_{\text{CC}}^{(1,2,3)}$		$V_{\text{CC}}^{(1,2h)}$		$V_{\text{CC}}^{(1,2h)} + V_{\text{DFT}}^{(2s)}$		$V_{\text{CC}}^{(1)} + V_{\text{DFT}}^{(2)}$		
1	608	7	606	6	596	-3	609	9	602	2	601	1	600
2	614	9	610	7	600	-3	615	12	604	1	605	2	603
3	786	62	759	37	726	4	836	114	711	-11	724	3	722
4	791	47	781	36	747	3	855	110	738	-7	744	-1	745
5	880	57	872	35	835	-2	880	42	830	-8	823	-15	838
6	881	29	874	10	860	-4	888	24	853	-11	851	-13	864
7	888	14	878	8	868	-2	941	70	874	4	874	3	870
8	911	29	888	15	878	5	962	89	882	9	881	8	873
9	1020	26	1001	6	994	-1	1035	40	990	-5	994	-1	995
10	1069	27	1053	10	1041	-2	1075	32	1039	-3	1042	-1	1043
11	1086	9	1071	4	1067	0	1085	18	1064	-3	1077	10	1067
12	1164	21	1146	6	1139	-1	1174	34	1138	-2	1144	3	1140
13	1223	44	1189	8	1183	2	1220	39	1195	14	1179	-2	1181
14	1300	45	1274	7	1265	-1	1314	48	1275	8	1256	-11	1267
15	1421	27	1395	10	1383	-2	1421	37	1390	6	1394	10	1385
16	1523	38	1495	5	1495	5	1520	30	1492	2	1485	-5	1491
17	1599	36	1566	9	1557	0	1589	32	1561	4	1563	6	1558
18	3259	140	3066	-64	3103	-27	3144	14	3120	-10	3120	-10	3130
19	3267	138	3095	-45	3124	-16	3155	15	3126	-14	3129	-11	3140
20	3308	153	3094	-66	3143	-17	3175	14	3155	-6	3155	-6	3161
21	3337	162	3156	-13	3147	-22	3182	12	3173	3	3175	6	3169
	MAD	53		19		6		40		6		6	
	MAX	162		66		27		114		14		15	

<sup>a</sup> – experimental values references in Ref.<sup>[76]</sup>

error is reduced by a factor of 3–4 compared to normal modes. This reduction of the error is especially pronounced for the modes that are well localizable, in particular for modes 3–6 and modes 18–21 (cf. Fig. 3). Note that in terms of localized-mode coordinates, such a hybrid PES can provide results that are as accurate as the full CC PES including three-mode potentials expanded in normal-mode coordinates.

As a further approximation, the off-diagonal elements of Hessian in the basis of localized modes are used to calculate harmonic two-mode potentials. These can be used to replace the full anharmonic two-mode potential for the modes belonging to the same subset in the localization. This simplified hybrid PES is denoted as  $V_{\text{CC}}^{(1,2\text{h})} + V_{\text{DFT}}^{(2\text{s})}$ . This way, 32 two-mode potentials (corresponding to 8 192 single-point calculations) can be omitted. Such an approximation results in an MAD of the fundamental frequencies of  $6 \text{ cm}^{-1}$  and a maximum deviation of  $14 \text{ cm}^{-1}$  which is identical to the accuracy obtained when included all DFT two-mode potentials.

Finally, as a low-cost approximation we use only the harmonic two-mode potentials along with anharmonic one-mode potentials, both expanded in localized-mode coordinates, which requires only 336 single-point CCSD(T)-F12b/cc-pVTZ-F12 calculations. This PES is denoted as  $V_{\text{CC}}^{(1,2\text{h})}$ . This computationally very cheap approach results in an MAD of  $40 \text{ cm}^{-1}$ , and a maximal deviation of  $114 \text{ cm}^{-1}$ . It is noteworthy that the C–H stretching vibrations are very well reproduced and are only about  $14 \text{ cm}^{-1}$  off from the experimental values. This is a closer agreement than for the full  $V_{\text{CC}}^{(1,2,3)}$  PES expanded in normal-mode coordinates. If normal-mode coordinates are used, we can obtain the anharmonic one-mode potentials ( $V_{\text{CC}}^{(1)}$ ) with the same computational effort. As in the ethene example, this results in rather large discrepancies for the C–H stretching modes, whereas for the other vibrations, the deviations are at the similar as for localized modes. All in all, the MAD raises to  $53 \text{ cm}^{-1}$ , and the maximal deviation to  $162 \text{ cm}^{-1}$  when applying this low-cost approximation with normal-mode coordinates instead of localized-mode

coordinates.

In summary, for furan similar trends as in the ethene example are observed. In particular, for the modes that can be well localized, such as the C–H stretching and (to a smaller extent) bending vibrations, the convergence of the  $n$ -mode expansion is significantly faster in localized-mode coordinates. This makes it possible to employ computationally cheaper hybrid potential energy surfaces. If localized-mode coordinates are used, a hybrid  $V_{\text{CC}}^{(1)} + V_{\text{DFT}}^{(2)}$  yields fundamental vibrational frequencies of the same accuracy as a  $V_{\text{CC}}^{(1,2,3)}$  expanded in normal-mode coordinates. Moreover, in localized-mode coordinates it becomes possible to neglect some of the two-mode potentials by replacing them with the harmonic counterparts arising from the localization without loss of accuracy. Finally, localized-mode coordinates are better suited for devising low-cost approximations that require only the calculation of anharmonic one-mode potentials and that can provide a first approximation of anharmonic corrections.

## 8 Conclusions and summary

In this paper, we have presented L-VSCF/L-VCI calculations performed for all fundamental vibrations in two prototypical small molecules, ethene and furan. We have investigated to what extent employing localized-mode coordinates instead of the conventionally used normal-mode coordinates can be beneficial with respect to the main bottlenecks of such anharmonic vibrational calculations.

Concerning the convergence of the  $n$ -mode expansion, we observe a significantly faster convergence in localized-mode coordinates. While for ethene, the inclusion of up to four mode potentials is required to reduce the mean average deviation from the experimental fundamental frequencies below  $10 \text{ cm}^{-1}$  when using normal-mode coordinates, with localized-mode coordinates the same level of accuracy can already be reached with only

up to three-mode potentials. Similarly, for furan it is possible to approximate the two-mode potentials with lower-level DFT calculations when using localized-mode coordinates, while still achieving the same level of accuracy as with a high-level CCSD(T)-F12x PES including up to three-mode potentials in terms of normal-mode coordinates. Moreover, we observe that the two-mode couplings are significantly reduced in localized-mode coordinates, in particular within the subsets of modes that are used in the localization procedure. This can be exploited to neglect selected two-mode potentials or to replace them by their harmonic counterparts, without losing accuracy for the fundamental frequencies. In combination, these advantageous features of localized-mode coordinates can vastly reduce the number of single-point calculations needed to construct the PES and thus help to alleviate this computational bottleneck.

In addition, we find that the convergence with respect to the VCI excitation space proceeds more smoothly when using localized-mode coordinates. This could be exploited to reduce the computational effort required for this step, for instance by making schemes for the selection of the relevant excitations<sup>[18-21]</sup> more efficient. Moreover, as the error with small VCI excitation spaces is significantly reduced when using localized-mode coordinates, it becomes possible to devise low-cost models that can give a first estimate of anharmonic frequency corrections. For our two test cases, we find that L-VCI-S with only anharmonic one-mode potentials and harmonic two-mode potentials can provide such a qualitatively correct estimate for all fundamental vibrations, whereas with normal-mode coordinates, at least anharmonic two-mode potentials in combination with a significantly larger excitation space would be required.

While similar benefits can also be achieved with optimized coordinates,<sup>[34-37]</sup> localized-mode coordinates offer the advantage that they can be constructed *a priori*, i.e., no anharmonic PES is required for their construction. Moreover, compared to other local coordinates<sup>[27,28,30]</sup> or local (curvilinear) internal coordinates<sup>[23,24]</sup> that could be employed

to achieve such benefits in anharmonic vibrational calculations, the rigorously-defined localized modes used here do not require the manual *ad hoc* construction of vibrational coordinates. Instead, only a chemically meaningful assignment of the normal modes to subsets is required as prerequisite for the localization procedure. The effect that the choice of these subsets has on the accuracy of the anharmonic vibrational frequencies will be subject of our future work.

Thus, our results demonstrate that normal modes may not always be optimal for anharmonic vibrational calculations. In particular for well-localizable vibrations, such as C–H stretching and bending modes, localized modes are in general a better choice. The benefits of localized modes will become more pronounced with increasing size of the molecule, for which a better localization will be possible and for which further criteria, such as distance cut-offs,<sup>[46]</sup> can be applied. Finally, the strategies presented here are not limited to the calculation of fundamental frequencies, but will also be applicable when targeting overtones and combination bands. This will be addressed in our future work.

## Acknowledgments

CRJ is grateful to the Deutsche Forschungsgemeinschaft (DFG) for funding via grant JA 2329-2/1. PTP would like to thank Prof. Wim Klopper for his kind hospitality in his group at the Karlsruhe Institute of Technology (KIT).

## References

- [1] F. Pfeiffer, G. Rauhut, D. Feller, and K. A. Peterson, *J. Chem. Phys.* **138**, 044311 (2013).
- [2] J. Bloino, M. Biczysko, and V. Barone, *J. Phys. Chem. A* **119**, 11862 (2015).

- [3] A. Tajti, P. G. Szalay, A. G. Császár, M. Kállay, J. Gauss, E. F. Valeev, B. A. Flowers, J. Vázquez, and J. F. Stanton, *J. Chem. Phys.* **121**, 11599 (2004).
- [4] V. Barone, *J. Chem. Phys.* **122**, 014108 (2005).
- [5] Y. Cornaton, M. Ringholm, O. Louant, and K. Ruud, *Phys. Chem. Chem. Phys.* (2016).
- [6] O. Christiansen, *Phys. Chem. Chem. Phys.* **14**, 6672 (2012).
- [7] T. K. Roy and R. B. Gerber, *Phys. Chem. Chem. Phys.* **15**, 9468 (2013).
- [8] J. O. Jung and R. B. Gerber, *J. Chem. Phys.* **105**, 10332 (1996).
- [9] S. Carter, J. M. Bowman, and N. C. Handy, *Theor. Chem. Acc.* **100**, 191 (1998).
- [10] D. M. Benoit, *J. Chem. Phys.* **120**, 562 (2003).
- [11] L. Pele and R. B. Gerber, *J. Chem. Phys.* **128**, 165105 (2008).
- [12] G. Rauhut, *J. Chem. Phys.* **121**, 9313 (2004).
- [13] K. Yagi, S. Hirata, and K. Hirao, *Theor. Chem. Acc.* **118**, 681 (2007).
- [14] P. Seidler, T. Kaga, K. Yagi, O. Christiansen, and K. Hirao, *Chem. Phys. Lett.* **483**, 138 (2009).
- [15] T. Hrenar, H.-J. Werner, and G. Rauhut, *Phys. Chem. Chem. Phys.* **7**, 3123 (2005).
- [16] C. Puzzarini, M. Biczysko, and V. Barone, *J. Chem. Theory Comput.* **6**, 828 (2010).
- [17] J. M. Bowman, K. Christoffel, and F. Tobin, *J. Phys. Chem.* **83**, 905 (1979).
- [18] G. Rauhut, *J. Chem. Phys.* **127**, 184109 (2007).
- [19] Y. Scribano and D. M. Benoit, *Chem. Phys. Lett.* **458**, 384 (2008).
- [20] P. Carbonnière, A. Dargelos, and C. Pouchan, *Theor. Chem. Acc.* **125**, 543 (2010).

- [21] C. König and O. Christiansen, *J. Chem. Phys.* **142**, 144115 (2015).
- [22] A. G. Császár and N. C. Handy, *J. Chem. Phys.* **102**, 3962 (1995).
- [23] S. N. Yurchenko, W. Thiel, and P. Jensen, *J. Mol. Spectrosc.* **245**, 126 (2007).
- [24] Y. Scribano, D. M. Lauvergnat, and D. M. Benoit, *J. Chem. Phys.* **133**, 094103 (2010).
- [25] J. Pesonen, K. O. E. Henriksson, J. R. López-Blanco, and P. Chacón, *J Math Chem* **50**, 1521 (2012).
- [26] B. R. Henry, *Acc. Chem. Res.* **10**, 207 (1977).
- [27] G. R. Low and H. G. Kjaergaard, *J. Chem. Phys.* **110**, 9104 (1999).
- [28] T. Salmi, H. G. Kjaergaard, and L. Halonen, *J. Phys. Chem. A* **113**, 9124 (2009).
- [29] D. L. Howard, P. Jørgensen, and H. G. Kjaergaard, *J. Am. Chem. Soc.* **127**, 17096 (2005).
- [30] Y. Wang and J. M. Bowman, *Chem. Phys. Lett.* **491**, 1 (2010).
- [31] J. S. Mancini and J. M. Bowman, *J. Chem. Phys.* **139**, 164115 (2013).
- [32] Y. Wang and J. M. Bowman, *J. Chem. Phys.* **136**, 144113 (2012).
- [33] C. König, M. B. Hansen, I. H. Godtliobsen, and O. Christiansen, *J. Chem. Phys.* **144**, 074108 (2016).
- [34] T. C. Thompson and D. G. Truhlar, *J. Chem. Phys.* **77**, 3031 (1982).
- [35] N. Moiseyev, *Chem. Phys. Lett.* **98**, 233 (1983).
- [36] K. Yagi, M. Keçeli, and S. Hirata, *J. Chem. Phys.* **137**, 204118 (2012).
- [37] B. Thomsen, K. Yagi, and O. Christiansen, *J. Chem. Phys.* **140**, 154102 (2014).

- [38] K. Yagi and H. Otaki, *J. Chem. Phys.* **140**, 084113 (2014).
- [39] Ch. R. Jacob and M. Reiher, *J. Chem. Phys.* **130**, 084106 (2009).
- [40] Ch. R. Jacob, S. Lubner, and M. Reiher, *J. Phys. Chem. B* **113**, 6558 (2009).
- [41] Ch. R. Jacob, S. Lubner, and M. Reiher, *Chem. Eur. J.* **15**, 13491 (2009).
- [42] V. Liégeois, Ch. R. Jacob, B. Champagne, and M. Reiher, *J. Phys. Chem. A* **114**, 7198 (2010).
- [43] T. Weymuth, Ch. R. Jacob, and M. Reiher, *J. Phys. Chem. B* **114**, 10649 (2010).
- [44] Ch. R. Jacob, *ChemPhysChem* **12**, 3291 (2011).
- [45] P. T. Panek and Ch. R. Jacob, *ChemPhysChem* **15**, 3365 (2014).
- [46] X. Cheng and R. P. Steele, *J. Chem. Phys.* **141**, 104105 (2014).
- [47] M. W. D. Hanson-Heine, *J. Chem. Phys.* **143**, 164104 (2015).
- [48] E. L. Klinting, C. König, and O. Christiansen, *J. Phys. Chem. A* **119**, 11007 (2015).
- [49] J. K. G. Watson, *Mol. Phys.* **15**, 479 (1968).
- [50] M. Neff, T. Hrenar, D. Oschetzki, and G. Rauhut, *J. Chem. Phys.* **134**, 064105 (2011).
- [51] O. Christiansen, *J. Chem. Phys.* **120**, 2149 (2004).
- [52] O. Christiansen and J. M. Luis, *Int. J. Quantum Chem.* **104**, 667 (2005).
- [53] G. Rauhut et al., Database of potential energy surfaces, <http://pes-database.theochem.uni-stuttgart.de/>, Accessed: 23.02.2016.
- [54] T. B. Adler, G. Knizia, and H.-J. Werner, *J. Chem. Phys.* **127**, 221106 (2007).
- [55] G. Knizia, T. B. Adler, and H.-J. Werner, *J. Chem. Phys.* **130**, 054104 (2009).



- [56] K. A. Peterson, T. B. Adler, and H.-J. Werner, *J. Chem. Phys.* **128**, 084102 (2008).
- [57] T. Weymuth, M. P. Haag, K. Kiewisch, S. Lubner, S. Schenk, Ch. R. Jacob, C. Herrmann, J. Neugebauer, and M. Reiher, *J. Comput. Chem.* **33**, 2186–2198 (2012).
- [58] H.-J. Werner et al., Molpro, version 2012.1, a package of ab initio programs, 2012, see <http://www.molpro.net>.
- [59] R. Ahlrichs et al., TURBOMOLE, URL: <http://www.turbomole.com>.
- [60] R. Ahlrichs, M. Bär, M. Häser, H. Horn, and C. Kölmel, *Chem. Phys. Lett.* **162**, 165 (1989).
- [61] A. D. Becke, *Phys. Rev. A* **38**, 3098 (1988).
- [62] J. P. Perdew, *Phys. Rev. B* **33**, 8822 (1986).
- [63] F. Weigend and R. Ahlrichs, *Phys. Chem. Chem. Phys.* **7**, 3297 (2005).
- [64] K. Eichkorn, O. Treutler, H. Öhm, M. Häser, and R. Ahlrichs, *Chem. Phys. Lett.* **240**, 283 (1995).
- [65] F. Weigend, *Phys. Chem. Chem. Phys.* **8**, 1057 (2006).
- [66] C. R. Jacob, S. M. Beyhan, R. E. Bulo, A. S. P. Gomes, A. W. Götz, K. Kiewisch, J. Sikkema, and L. Visscher, *Journal of Computational Chemistry* **32**, 2328 (2011).
- [67] T. E. Oliphant, *Computing in Science & Engineering* **9**, 10 (2007).
- [68] T. Oliphant et al., NUMPY — A python library for numerical computations, URL: <http://www.scipy.org/NumPy>.
- [69] J. M. L. Martin and P. R. Taylor, *Chem. Phys. Lett.* **248**, 336 (1996).
- [70] J. Neugebauer and B. A. Hess, *J. Chem. Phys.* **118**, 7215 (2003).

- [71] E. D. Simandiras, N. C. Handy, and R. D. Amos, *J. Phys. Chem.* **92**, 1739 (1988).
- [72] R. Burcl, N. C. Handy, and S. Carter, *Spectrochimica Acta Part A: Molecular and Biomolecular Spectroscopy* **59**, 1881 (2003).
- [73] V. Barone, *Chemical Physics Letters* **383**, 528 (2004).
- [74] P. Daněček and P. Bouř, *J. Comput. Chem.* **28**, 1617 (2007).
- [75] M. Biczysko, P. Panek, G. Scalmani, J. Bloino, and V. Barone, *J. Chem. Theory Comput.* **6**, 2115 (2010).
- [76] F. Billes, H. Böhlig, M. Ackermann, and M. Kudra, *J. Mol. Struct.: THEOCHEM* **672**, 1 (2004).